Turkish J. Eng. Env. Sci.
36 (2012) , 208 – 218.

doi:10.3906/muh-1110-5

# Electro-thermo-mechanical creep and time-dependent behavior of FGPM spheres

**Ali GHORBANPOUR ARANI*, Reza KOLAHCHI, Ali Akbar MOSALLAIE BARZOKI, Abbas LOGHMAN**
*Faculty of Mechanical Engineering, University of Kashan, Kashan-IRAN*
*e-mails: aghorban@kashanu.ac.ir, aghorbanpour@yahoo.com*

Received: 18.10.2011

**Abstract**

Piezoelectric materials exhibit significant creep effects even at room temperature. History of stresses and electric potential of thick-walled spheres made of functionally graded piezoelectric material (FGPM) subjected to an internal pressure and a distributed temperature was investigated. A semi-analytical method in conjunction with the method of successive approximation was developed. A major redistribution for electric potential was found to take place throughout the thickness, which changes with time in the same direction as the compressive radial stress. The results of this investigation can be used to improve the accuracy and reliability of smart structures used for high-precision applications.

**Key Words:** Time-dependent, electro-thermo-mechanical creep, FGPM sphere

## 1. Introduction

The best known among the smart materials are certainly the piezoelectric materials and more precisely the piezoceramics (PZT). When an electric field is applied to these materials, it results in mechanical stress or strain. Such bidirectional application makes these materials ideal for use as both sensors (direct effect) and actuators (converse effects). Applications of functionally graded materials (FGMs) have recently been attracted researchers' attention in such fields as nuclear, aircraft, space engineering, sensors, actuators, armor, photodetectors, and pressure vessels.

Elastic analysis of FGPM spheres and cylinders under mechanical, electrical, thermal, and magnetic loads has been considered by many investigators. Stress and electric potential fields in piezoelectric smart spheres were presented by Ghorbanpour Arani et al. (2006). Wang and Xu (2010) studied the effect of material inhomogeneity on electromechanical behaviors of functionally graded piezoelectric spherical structures. Effect of material in-homogeneity on electro-thermo-mechanical behaviors of functionally graded piezoelectric rotating cylinder was considered by Ghorbanpour Arani et al. (2011a). Electro-thermo-mechanical behaviors of FGPM spheres were studied by Ghorbanpour Arani et al. (2011b) by analytical method and ANSYS software. Dai and Wang (2005) presented the thermo-electro-elastic transient responses in piezoelectric hollow structures.

*Corresponding author

Although the elastic behavior of hollow FGPM structures is well established, few publications about time-dependent creep behavior of spheres and cylinders can be found in the literature. You et al. (2007) considered steady state creep deformation and stresses in thick-walled cylindrical vessels of FGM subjected to internal pressure. Loghman and Shokouhi (2009) evaluated creep damages of thick-walled spheres using a long-term creep constitutive model. Time-dependent deformation and fracture of multi-material systems at high temperature were presented by Xuan et al. (2009). They considered a thick-walled sphere of FGM material subjected to internal pressure. Tejeet and Gupta (2011) investigated the effect of anisotropy on steady-state creep in functionally graded cylinder. Recently magnetothermoelastic creep analysis of functionally graded cylinder was presented by Loghman et al. (2010). Semi-analytical solution of time-dependent electro-thermo-mechanical creep for radially polarized piezoelectric cylinder was investigated by Ghorbanpour Arani et al. (2011c). Due to time-dependent creep deformation of FGPM structures the accuracy and reliability of smart structures must be reconsidered. It has been shown by Zhou and Kamlah (2006) that even at room temperature ferroelectric piezoceramics exhibit significant creep effects. However, the time-dependent creep response of FGPM components has not yet been investigated. The main objective of the present study was to show the significant effect of creep on stresses and electric potential redistributions during the life of a smart sphere.

## 2. Electromechanical coupling

Stresses $\sigma$ and strains $\varepsilon$ from the mechanical point of view, as well as flux density $D$ and field strength $E$ from the electrostatic point of view, may be arbitrarily combined as follows: (Ghorbanpour Arani et al., 2011a)

$$\left\{ \begin{array}{c} \sigma \\ D \end{array} \right\} = \left[ \begin{array}{cc} C^E & -e \\ e^T & \in^{\varepsilon} \end{array} \right] \left\{ \begin{array}{c} \varepsilon \\ E \end{array} \right\}, \tag{1}$$

where $C^E$, $\in^{\varepsilon}$, $e$, and $e^T$ represent the fourth-order elasticity tensor, the dielectric permittivity tensor, third order tensor of piezoelectric coefficient, and its transpose, respectively. Electric field tensor $E$ could be written in terms of electric potential $\phi$ (Ghorbanpour Arani et al., 2011b)

$$E = -grad\ \phi. \tag{2}$$

## 3. Formulation for electro-thermo-elastic creep response of FGPM spheres

A hollow FGPM sphere with an inner radius $a$ and outer radius $b$ is considered. The radially polarized sphere is subjected to an internal pressure $P_a$, an electric potential $\phi$ and a distributed temperature field $T(r)$ (Figure 1). A spherical coordinate system $(r, \theta, \varphi)$ or $(1, 2, 3)$ with the origin identical to the center of a hollow sphere is used. For the spherically symmetric problem, we have $u_\theta = u_\varphi = 0, u_r = u_r(r)$ and electric potential $(\phi)$ are the functions of radial coordinates. It is appropriate to introduce the following dimensionless quantities:

$$\sigma_i = \frac{\sigma_{ii}}{C_{22}}\ (i = r, \theta) \quad , \quad C_i = \frac{C_{ri}}{C_{\theta\theta}}\ (i = r, \theta), \quad C_\varphi = \frac{C_{\theta\varphi}}{C_{\theta\theta}}, E_i = \frac{e_{ri}}{E_0}\ (i = r, \theta, \varphi), \quad E_0 = \sqrt{C_{\theta\theta} \in_{rr}},$$

$$\xi = \frac{r}{a}, \quad U_\xi = \frac{u_r}{a} \quad , \quad \eta = \frac{b}{a} \quad , \quad \Phi = \frac{\phi}{\phi_0}, \quad \phi_0 = a\sqrt{\frac{C_{\theta\theta}}{\in_{rr}}}, \quad D_r = \frac{D_{rr}}{E_0}. \tag{3}$$

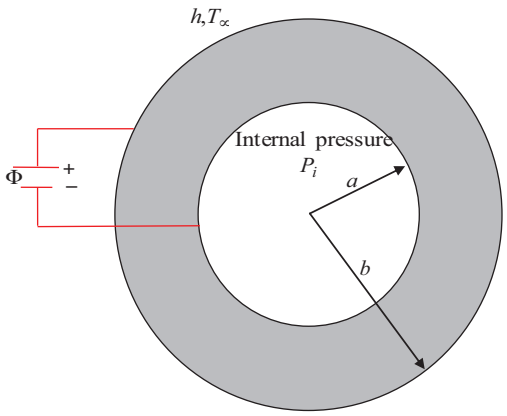


**Figure 1.** Hollow FGPM sphere subjected to an internal pressure, thermal loading, and applied voltage $\Phi$.

Using these dimensionless variables, the equilibrium equation of the FGPM sphere in the absence of body force, Maxwell's equation for free electric charge density, the radial and circumferential strains, and the relation between electric field and electric potential are reduced to

$$\frac{\partial \sigma_r}{\partial \xi} + \frac{2\left(\sigma_r - \sigma_\theta\right)}{\xi} = 0, \tag{4}$$

$$\frac{\partial D_r}{\partial \xi} + \frac{2D_r}{\xi} = 0. \tag{5}$$

$$\varepsilon_r = \frac{\partial u_\xi}{\partial \xi}, \varepsilon_\theta = \varepsilon_\zeta = \frac{u_\xi}{\xi}, \tag{6}$$

$$E_r = -\frac{\partial \Phi}{\partial \xi}. \tag{7}$$

Appropriate power functions for all properties are assumed as (Ghorbanpour Arani, 2011c):

$$\Psi_r = \Psi_0 \left(\xi\right)^\gamma, \tag{8}$$

in which $\Psi_r$ represents the general properties of the sphere such as the elastic, piezoelectric, and dielectric coefficients and thermal conductivity, $\Psi_0$ corresponds to the value of the coefficients at the outer surface, and $\gamma$ is the material's in-homogeneity parameter. Using Eqs. (3)-(8), the 2 components of the stress and the radial electric (Eq. (1)) displacement yield: (Mendelson, 1968; Salehi-Khojin and Jalili, 2008)

$$\left\{ \begin{array}{c} \sigma_r \\ \sigma_\theta \end{array} \right\} = \xi^\gamma \left( \left[ \begin{array}{ccc} C_r & C_\theta & C_\theta \\ C_\theta & 1 & C_\varphi \end{array} \right] \left( \left\{ \begin{array}{c} \frac{\partial U_\xi}{\partial \xi} \\ \frac{U_\xi}{\xi} \\ \frac{U_\xi}{\xi} \end{array} \right\} - \xi^\gamma \left\{ \begin{array}{c} \alpha_r \\ \alpha_\theta \\ \alpha_\theta \end{array} \right\} T\left(\xi\right) - \left\{ \begin{array}{c} \varepsilon_r^c \\ \varepsilon_\theta^c \\ \varepsilon_\theta^c \end{array} \right\} \right) + \left[ \begin{array}{c} E_r \\ E_\theta \end{array} \right] \left\{ \frac{\partial \Phi}{\partial \xi} \right\} \right), \tag{9}$$

$$\left\{D_r\right\} = \xi^\gamma \left( \left[ \begin{array}{ccc} E_r & E_\theta & E_\theta \end{array} \right] \left( \left\{ \begin{array}{c} \frac{\partial U_\xi}{\partial \xi} \\ \frac{U_\xi}{\xi} \\ \frac{U_\xi}{\xi} \end{array} \right\} - \xi^\gamma \left\{ \begin{array}{c} \alpha_r \\ \alpha_\theta \\ \alpha_\theta \end{array} \right\} T\left(\xi\right) - \left\{ \begin{array}{c} \varepsilon_r^c \\ \varepsilon_\theta^c \\ \varepsilon_\theta^c \end{array} \right\} \right) - \left\{ \frac{\partial \Phi}{\partial \xi} \right\} \right). \tag{10}$$

The solution of Eq. (5) is:

$$D_r = \frac{A_1}{\xi^2}, \tag{11}$$

where $A_1$ is a constant. Substituting Eq. (11) into Eq. (10) and combining with Eq. (9), we obtain:

$$\begin{Bmatrix} \sigma_r \\ \sigma_\theta \end{Bmatrix} = \xi^{\gamma} \left( \begin{bmatrix} C_r & C_\theta & C_\theta \\ C_\theta & 1 & C_\varphi \end{bmatrix} \left( \begin{Bmatrix} \frac{\partial U_\xi}{\partial \xi} \\ \frac{U_\xi}{\xi} \\ \frac{U_\xi}{\xi} \end{Bmatrix} - \xi^{\gamma} \begin{Bmatrix} \alpha_r \\ \alpha_\theta \\ \alpha_\theta \end{Bmatrix} T(\xi) - \begin{Bmatrix} \varepsilon_r^c \\ \varepsilon_\theta^c \\ \varepsilon_\theta^c \end{Bmatrix} \right) \right.$$
$$\left. + \begin{bmatrix} E_r \\ E_\theta \end{bmatrix} \left( \begin{bmatrix} E_r & E_\theta & E_\theta \end{bmatrix} \left( \begin{Bmatrix} \frac{\partial U_\xi}{\partial \xi} \\ \frac{U_\xi}{\xi} \\ \frac{U_\xi}{\xi} \end{Bmatrix} - \xi^{\gamma} \begin{Bmatrix} \alpha_r \\ \alpha_\theta \\ \alpha_\theta \end{Bmatrix} T(\xi) - \begin{Bmatrix} \varepsilon_r^c \\ \varepsilon_\theta^c \\ \varepsilon_\theta^c \end{Bmatrix} \right) - A_1 \xi^{-\gamma-2} \right) \right). \tag{12}$$

In our study a distributed temperature field due to steady-state heat conduction was considered. Using Eq. (8) for the thermal conductivity property, the heat conduction equation without any heat source is written in spherical coordinate as (Ghorbanpour Arani et al., 2011a):

$$\frac{1}{\xi^2} \left( K_0 \, \xi^{\gamma+2} \, T'(\xi) \right)' = 0, \tag{13}$$

where () denotes differentiation with respect to $\xi$ and $K_0$ is the nominal heat conductivity coefficient. Integrating Eq. (13) yields:

$$T(\xi) = -\frac{B_1}{\gamma+1} \xi^{-\gamma-1} + B_2, \tag{14}$$

constants $B_1$ and $B_2$ are obtained using the thermal boundary condition.

Finally, combination of Eqs. (12) and (14) and substituting into Eq. (4) yield the following non-homogeneous Cauchy differential equation:

$$\xi^2 \frac{\partial^2 U_\xi}{\partial \xi^2} + D_1 \xi \frac{\partial U_\xi}{\partial \xi} + D_2 U_\xi = D_4 B_1 + (D_6 \varepsilon_r^c + D_7 \varepsilon_\theta^c)\xi + \left( \frac{\partial \varepsilon_r^c}{\partial \xi} + D_8 \frac{\partial \varepsilon_\theta^c}{\partial \xi} \right) \xi^2 + D_5 B_2 \xi^{(1+\gamma)} + D_3 A_1 \xi^{-(1+\gamma)} \tag{15}$$

where $D_k$ $(k = 1, ...8)$ are defined in Appendix A.

### 3.1. Electro-thermo-elastic analysis of FGPM spheres

A semi-analytical method for solution of this differential equation was employed. In this method the solution domain is divided into some finite divisions as shown in Figure 2. The coefficients of Eq. (15) are evaluated at $\xi^m$, mean radius of $m^{th}$ division and the differential equation with constant coefficients valid only in the $m^{\text{th}}$ sub-domain is rewritten as follows (Kordkheili and Naghdabadi, 2007):

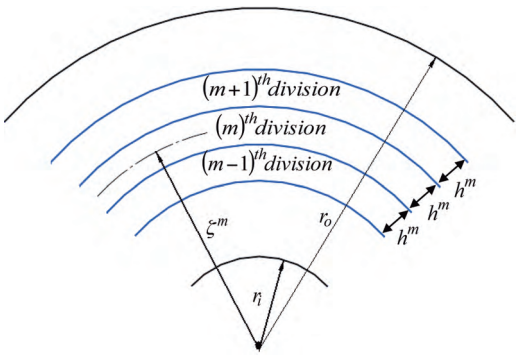


**Figure 2.** Dividing radial domain into some finite sub-domains.

$$\left(P_1^m \frac{d^2}{dr^2} + P_2^m \frac{d}{dr} + P_3^m\right) U_\xi^m + P_4^m = 0, \tag{16}$$

$$P_1^m = (\xi^m)^2, \tag{17}$$

$$P_2^m = D_1 \xi^m, \tag{18}$$

$$P_3^m = D_2, \tag{19}$$

$$\begin{aligned} P_4^m = D_4 B_1 + \left(D_6\, \varepsilon_r^c|_{\xi=\xi^m} + D_7\, \varepsilon_\theta^c|_{\xi=\xi^m}\right) \xi^m + \left(D_8\, \frac{\partial \varepsilon_r^c}{\partial \xi}\bigg|_{\xi=\xi^m} + D_9\, \frac{\partial \varepsilon_\theta^c}{\partial \xi}\bigg|_{\xi=\xi^m}\right) (\xi^m)^2 \\ + D_5 B_2 (\xi^m)^{\,(1+\gamma)} + D_3 A_1 (\xi^m)^{\,-(1+\gamma)}. \end{aligned} \tag{20}$$

The coefficients of Eq. (16) are evaluated in each division in terms of constants and the radius of the $m^{th}$ division. The exact solution for Eq. (16) is written as follows:

$$u_g^m = K_1^m \exp\left(\frac{-P_2^m + \sqrt{(P_2^m)^2 - 4P_3^m P_1^m}}{2P_1^m}\xi\right) + K_2^m \exp\left(\frac{-P_2^m - \sqrt{(P_2^m)^2 - 4P_3^m P_1^m}}{2P_1^m}\xi\right), \tag{21}$$

The particular solution of the differential Eq. (16) may be obtained as

$$u_p^m = -\xi^{q_1^m} \int \frac{\xi^{q_2^m}\, R(\xi)\,|_{\xi=\xi^m}}{W(q_1^m, q_2^m)|_{\xi=\xi^m}} + \xi^{q_2^m} \int \frac{\xi^{q_1^m}\, R(\xi)\,|_{\xi=\xi^m}}{W(q_1^m, q_2^m)|_{\xi=\xi^m}}, \tag{22}$$

in which $R(\xi)$is the expression on the right-hand side of Eq. (16) and $W(\xi)$ is defined as

$$W(q_1^m, q_2^m) = \begin{vmatrix} u_{g1}^m & u_{g2}^m \\ (u_{g1}^m)' & (u_{g2}^m)' \end{vmatrix}. \tag{23}$$

Combining Eqs. (20), (22), and (23) one can obtain the particular solution as

$$\begin{aligned} u_p^m = {} & \frac{\xi^4}{(q_2^m-4)(q_1^m-4)}\, \frac{\partial \varepsilon_r^c}{\partial \xi}\bigg|_{\xi=\xi^m} + \frac{D_8 \xi^4}{(q_2^m-4)(q_1^m-4)}\, \frac{\partial \varepsilon_\theta^c}{\partial \xi}\bigg|_{\xi=\xi^m} + \frac{D_6 \xi^3}{(q_2^m-4)(q_1^m-4)}\, \varepsilon_r^c|_{\xi=\xi^m} \\ & + \frac{D_7 \xi^3}{(q_2^m-4)(q_1^m-4)}\, \varepsilon_\theta^c|_{\xi=\xi^m} + \frac{D_3 \xi^{1-\gamma}}{(q_2^m+\gamma-1)(q_1^m+\gamma-1)} A_1^m + \frac{D_5 \xi^{3+\gamma}}{(3-q_2^m+\gamma)(3-q_1^m+\gamma)} B_2 \\ & + \frac{D_4 \xi^3}{(q_2^m-3)(q_1^m-3)} B_1. \end{aligned} \tag{24}$$

The complete solution for $U_\xi^m$ in terms of the non-dimensional radial coordinate is written as

$$U_\xi^m = u_g^m + u_p^m, \qquad \xi^m - \frac{h^m}{2} \le \xi \le \xi^m + \frac{h^m}{2}, \tag{25}$$

where $h^m$ is the thickness of the $m^{th}$ division and $K_1^m$ and $K_2^m$ are unknown constants for the $m^{th}$ division. The unknowns $K_1^m$, $K_2^m$, $A_1^m$, $A_2^m$, $B_1^m$, and $B_2^m$ are determined by applying the necessary boundary conditions between 2 adjacent sub-domains. For this purpose, the continuity of radial displacement, radial stress, and

electric potential are imposed at the interfaces of the adjacent sub-domains. These continuity conditions at the interfaces are

$$\begin{aligned}
&U_\xi^m\Big|_{\xi=\xi^m+\frac{h^m}{2}} = U_\xi^{m+1}\Big|_{\xi=\xi^{m+1}-\frac{h^{m+1}}{2}}, \quad \frac{dU_\xi^m}{d\xi}\Big|_{\xi=\xi^m+\frac{h^m}{2}} = \frac{dU_\xi^{m+1}}{d\xi}\Big|_{\xi=\xi^{m+1}-\frac{h^{m+1}}{2}},\\
&\sigma_r^m|_{\xi=\xi^m+\frac{h^m}{2}} = \sigma_r^{m+1}|_{\xi=\xi^{m+1}-\frac{h^{m+1}}{2}}, \quad \Phi^m|_{\xi=\xi^m+\frac{h^m}{2}} = \Phi^{m+1}|_{\xi=\xi^{m+1}-\frac{h^{m+1}}{2}}\\
&T_\xi^m\Big|_{\xi=\xi^m+\frac{h^m}{2}} = T_\xi^m\Big|_{\xi=\xi^{m+1}+\frac{h^{m+1}}{2}}, \quad \frac{\partial T_\xi^m}{\partial\xi}\Big|_{\xi=\xi^m+\frac{h^m}{2}} = \frac{\partial T_\xi^m}{\partial\xi}\Big|_{\xi=\xi^{m+1}+\frac{h^{m+1}}{2}},
\end{aligned} \tag{26}$$

and global boundary conditions are written in dimensionless form as

$$\sigma_r(1) = -1 \ , \sigma_r(\eta) = 0 \ \ , \phi(1) = 0 \ \ , \phi(\eta) = 0. \tag{27}$$

It must be noted that in this case the FGPM hollow sphere is subjected to an internal uniform pressure and zero electric potential (the direct piezoelectric effect) for which the sphere acts as a sensor.

The continuity conditions Eq. (26) together with the global boundary conditions Eq. (27) yield a set of linear algebraic equations in terms of $K_1^m$, $K_2^m, A_1^m$, $A_2^m$, $B_1^m$, and $B_2^m$. Solving the resultant linear algebraic equations the unknown coefficients are calculated. Then the displacement component, the stresses, and the electric potential are determined in each radial sub-domain. Increasing the number of divisions improves the accuracy of the results.

### 3.2. Time-dependent electro-thermo-elastic creep behavior of FGPM spheres

To obtain time-dependent stresses and electric potential, the creep strains must be considered. Creep strain rates are related to the material uniaxial creep constitutive model and the current stress tensor by the well-known Prandtl–Reuss relation. In this case the Prandtl-Reuss relation is written as (Mendelson, 1968)

$$\dot{\varepsilon}_r = \frac{\dot{\varepsilon}_e}{\sigma_e}\left[\sigma_r - \sigma_\theta\right], \quad \dot{\varepsilon}_\theta = \dot{\varepsilon}_\zeta = -\frac{\dot{\varepsilon}_r}{2}. \tag{28}$$

The Norton's creep constitutive model is considered to be (Penny and Marriott, 1995)

$$\dot{\varepsilon}_e^c = Y(\xi)\,\sigma_e^{n(\xi)}, \tag{29}$$

where $\dot{\varepsilon}_e^c$, $\sigma_e$, $Y(\xi)$, and $n(\xi)$ are the effective creep strain rate, effective stress, and radial-dependent material creep parameters. In this study $Y(\xi) = y_0\,\xi^{y_1}$ and $n(\xi)$ is considered to be a constant $n(\xi) = n_0$ and the Von Mises effective stress for spherical symmetry is written as

$$\sigma_e = \frac{1}{\sqrt{2}}\sqrt{(\sigma_\theta - \sigma_r)^2 + (\sigma_\theta - \sigma_\zeta)^2 + (\sigma_\zeta - \sigma_r)^2} \ = |\sigma_r - \sigma_\theta|\,. \tag{30}$$

To obtain history of stresses and electric potential a numerical procedure based on the method of successive approximation was tailored.

## 4. Numerical procedure to obtain history of stresses and electric potential

We have employed Mendelson's method of successive elastic solution to obtain history of stresses, displacement, and electric potential. It was shown that creep strains and their derivatives are involved in the non-homogenous part of differential Eq. (20) $P_4$. Immediately after loading the creep strains are zero and the solution is an elasticity problem. To solve differential Eq. (16) for a long time after loading, the method of successive elastic solution is used. The step-by-step procedure is explained in details as follows:

1- An appropriate time step is selected. In this solution the first time increment is selected as $\Delta t = 6\ month$. The total time is the sum of time increments as the creep process progresses in time. For the $i^{th}$ timing step the total time is $t_i = \sum_{k=1}^{i-1} \Delta t_k + \Delta t_i$

2- Thickness of the FGPM sphere is divided into $N$ equal divisions. Initial value of $\Delta\varepsilon^c_{r,im} = -0.00001$ for radial creep strain increments is estimated at all division points throughout the thickness. These are added to the accumulated creep strains obtained from the previous timing step at all division points throughout the FGPM sphere as

$$\varepsilon^c_{r,im} = \sum_{k=1}^{i-1} \Delta\varepsilon^c_{r,km} + \Delta\varepsilon^c_{r,im}, \quad \varepsilon^c_{\theta,im} = \sum_{k=1}^{i-1} \Delta\varepsilon^c_{\theta,km} + \Delta\varepsilon^c_{\theta,im}, \quad \Delta\varepsilon^c_{\theta,im} = \Delta\varepsilon^c_{\zeta,im} = -\frac{\Delta\varepsilon^c_{r,im}}{2},$$

where the subscripts $i$ and $m$ indicate the timing step and division point, respectively.

3- First and second order derivatives of radial and circumferential creep strains are calculated using finite difference approximation as follows (Mendelson, 1968):

$$\frac{\partial\varepsilon^c_{r,im}}{\partial\xi_m} = \frac{\varepsilon^c_{r,im+1} - \varepsilon^c_{r,im-1}}{2\ h^m}, \quad \frac{\partial\varepsilon^c_{\theta,im}}{\partial\xi_m} = \frac{\varepsilon^c_{\theta,im+1} - \varepsilon^c_{\theta,im-1}}{2\ h^m},$$

$$\frac{\partial^2\varepsilon^c_{r,im}}{(\partial\xi^2_m)} = \frac{\varepsilon^c_{r,im+1} - 2\varepsilon^c_{r,im} + \varepsilon^c_{r,im-1}}{(h^m)^2}, \quad \frac{\partial^2\varepsilon^c_{\theta,im}}{\partial\xi^2_m} = \frac{\varepsilon^c_{\theta,im+1} - 2\varepsilon^c_{\theta,im} + \varepsilon^c_{\theta,im-1}}{(h^m)^2}.$$

4- The accumulated creep strains and its first order derivatives are substituted in Eq. (16). This differential equation can be solved for the displacement at the $m^{th}$ layer. Then using second order derivatives stresses and electric potential are calculated at the same layer. Using local and global boundary conditions the displacements, stresses, and electric potentials at time $t_i$ are determined.

5- Effective stresses are then calculated at all division points as $\sigma_{e,im} = |\sigma_{r,im} - \sigma_{\theta,im}|$.

6- Effective creep strain rates are then calculated at all division points $(m)$ for the $i^{th}$ timing step using Norton's creep constitutive model as $\dot{\varepsilon}_{e,im} = Y(\xi_m)\,\sigma_{e,im}$

7- From the Prandtl-Reuss relation radial and circumferential creep strain rates are obtained as follows:

$$\dot{\varepsilon}_{r,im} = \frac{\dot{\varepsilon}_{e,im}}{\sigma_{e,im}}(\sigma_{r,im} - \sigma_{\theta,im}), \quad \dot{\varepsilon}_{\theta,im} = \dot{\varepsilon}_{\zeta,im} = -\frac{\dot{\varepsilon}_{r,im}}{2},$$

8- New values for radial and circumferential creep strain increments at all division points are then calculated using the above creep strain rates and the time increment as follows:

$$\Delta\varepsilon^{c,new}_{r,im} = \dot{\varepsilon}^c_{r,im} \times \Delta t_i, \quad \Delta\varepsilon^{c,new}_{\theta,im} = \dot{\varepsilon}^c_{\theta,im} \times \Delta t_i.$$

9- These newly obtained values for creep strain increments are compared with the initial estimated values at all division points for the convergence of the procedure. If convergence is obtained, time is advanced one increment and the procedure is repeated for the new time increment from step 1. If convergence is not satisfied, these newly obtained values of creep strain increments will be considered as initial values and the procedure will be repeated from step 2 until convergence is obtained.

## 5. Numerical results and discussion

The numerical results presented here are based on the mechanical ($C_{ij}$ $(i,j=r,\theta,\varphi)$), electrical ($e_{1i}$ $(i=r,\theta)$, $\in_{11}$), and thermal properties ($\alpha_r$,$\alpha_\theta$), which are defined for PZT_4 as follows (Jaffe and Berlincourt, 1965):

$$C_{rr}=115\,(GPa),\ \ C_{\theta\theta}=139\,(GPa),\ C_{\theta\varphi}=77.8\,(GPa),\ \ C_{r\theta}=74.3\,(GPa),\ e_{rr}=15.1\,(C/m^2),$$
$$e_{r\theta}=-5.2\,(C/m^2),\ \alpha_r=2\times10^{-5}(1/K),\quad \alpha_\theta=2\times10^{-6}(1/K),\ \ \in_{rr}=3.87\times10^{-9}\,(F/m)$$

The temperatures at the inner and outer surfaces of the FGPM sphere are considered to be $T_i=323K$ and $T_o=298K$, respectively, and the aspect ratio is$\eta=2$.

History of stresses and electric potential of the FGPM sphere for 2 different material properties identified by $\gamma=2$ and $\gamma=-2$ are reported in this paper. Radial and circumferential stress histories are illustrated in Figures 3 and 4 for the case $\gamma=2$ and in Figures 5 and 6 for the case$\gamma=-2$. In both cases radial stresses are constant with time at the inner and outer surfaces of the sphere satisfying the constant mechanical boundary conditions. Through-thickness radial stresses for the case $\gamma=-2$ are increasing with time at a decreasing rate so that there is a saturation condition beyond which not much change occurs. Indeed the solution approaches the steady state condition. For the case $\gamma=2$ through-thickness radial stress redistributions are decreasing with time and finally approach the steady state condition. Circumferential stresses for the case $\gamma=-2$ are decreasing at the inner surface of the FGPM sphere and increasing at the outer surface with decreasing rates so that they also approach steady state condition. For the case $\gamma=2$ through-thickness circumferential stress redistributions are increasing at the inner surface and decreasing at the outer surface of the sphere. Comparing stresses for the cases $\gamma=2$ and $\gamma=-2$ one can find that stresses are changing with time at a decreasing rate but in the opposite direction. Histories of the induced electric potentials are shown in Figures 7 and 8 for the

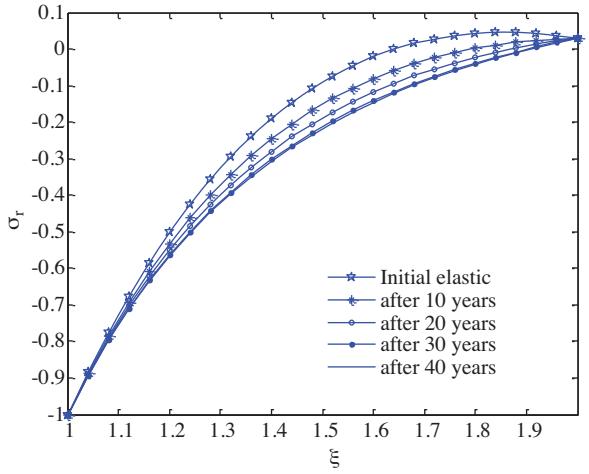


**Figure 3.** History of radial stress for the FGPM sphere from initial elastic up to 40 years for the case $\gamma=2$.

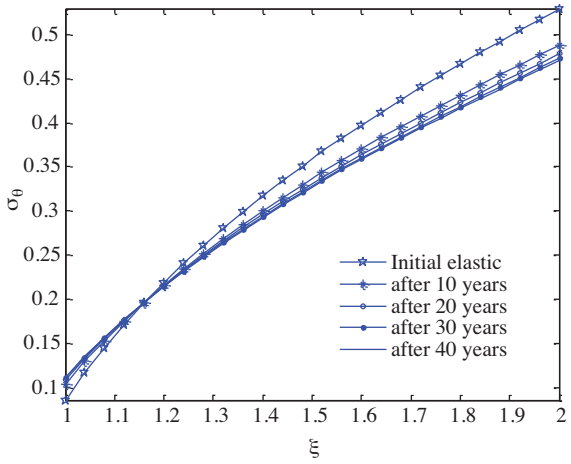


**Figure 4.** History of circumferential stress for the FGPM sphere from initial elastic up to 40 years for the case $\gamma=2$.

cases of $\gamma = 2$and $\gamma = -2$, respectively. For the case of $\gamma = -2$ the induced electric potential is increasing with time and approaches the steady state condition. For the case$\gamma = 2$ electric potential redistribution is in the opposite direction. In both cases the electric potential redistributions satisfy the electric boundary conditions at the inner and outer surfaces. However, through-thickness electric potentials are varying with time in the same direction as the compressive radial stress histories. Indeed, the electric potential histories are induced by the compressive radial stress histories during the life of the FGPM sphere.

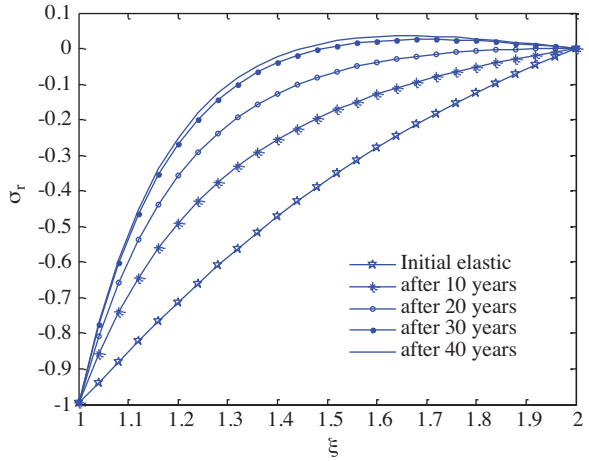


**Figure 5.** History of radial stress for the FGPM sphere from initial elastic up to 40 years for the case $\gamma = -2$.

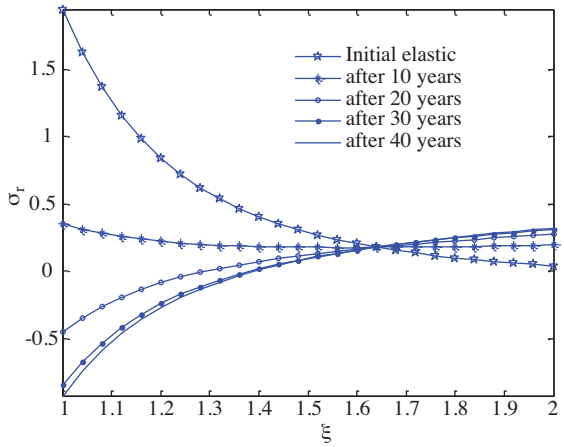


**Figure 6.** History of circumferential stress for the FGPM sphere from initial elastic up to 40 years for the case $\gamma = -2$.

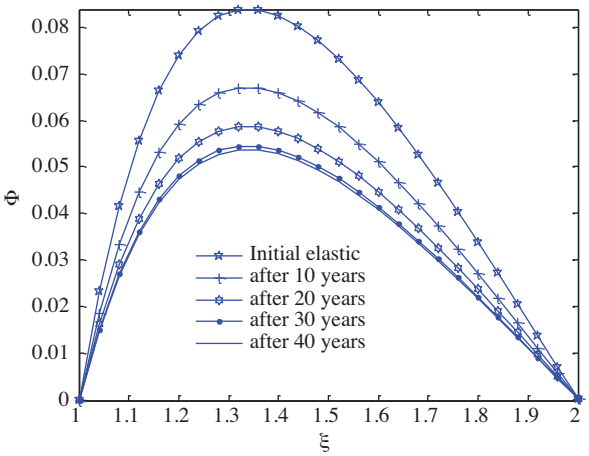


**Figure 7.** History of electric potential for the FGPM sphere from initial elastic up to 40 years for the case $\gamma = 2$.

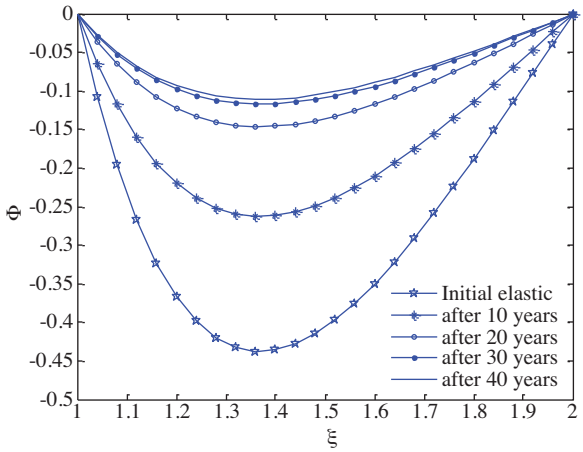


**Figure 8.** History of electric potential for the FGPM sphere from initial elastic up to 40 years for the case $\gamma = -2$.

## 6. Conclusions

Time-dependent creep behavior of a smart sphere was investigated to show the significant effect of creep on performance and reliability of smart structures used for high-precision applications. Time-dependent thermo-

electro-mechanical creep response of radially polarized FGPM hollow sphere is investigated using a semi-analytical numerical procedure. History of stresses and electric potentials of 2 different combinations of mechanical and electrical boundary conditions for 2 cases of the material in-homogeneity parameter $\gamma$ are studied. It was found that the stress and electric potential redistributions for $\gamma = -2$ are higher than those for $\gamma = 2$. In general, a major redistribution for stresses and electric potential take place throughout the thickness. Electric potentials are increasing with time in the same direction as the compressive radial stress histories. In fact, the electric potential histories are induced by the compressive radial stress histories during creep deformation of the FGPM sphere.

**Acknowledgment**

The authors are grateful to University of Kashan for supporting this work by Grant No. 65475/27.

## Appendix A

$$D_1 = \frac{\gamma\left(C_r+E_r^2\right)+2C_r+2E_r^2}{C_r+E_r^2}, \quad D_2 = \frac{\gamma(2C_\theta+2E_rE_\theta)+2C_\theta+2E_rE_\theta-2-2C_\varphi-4E_\theta^2}{C_r+E_r^2}, \quad D_3 = \frac{2E_\theta}{C_r+E_r^2},$$

$$D_4 = \frac{(\gamma+1)(2C_\theta\alpha_\theta+C_r\alpha_r+E_r(2E_\theta\alpha_\theta+E_r\alpha_r))+2(2C_\theta\alpha_\theta+C_r\alpha_r)+2(E_r-E_\theta)(2E_\theta\alpha_\theta+E_r\alpha_r)}{(C_r+E_r^2)(\gamma+1)} + \frac{((1+C_\varphi)\alpha_\theta+C_\theta\alpha_r)}{(C_r+E_r^2)(\gamma+1)}$$

$$D_5 = \frac{\gamma(4C_\theta\alpha_\theta-2C_r\alpha_r-2E_r(2E_\theta\alpha_\theta+E_r\alpha_r))-2(2C_\theta\alpha_\theta+C_r\alpha_r)-(2E_r-E_\theta)(2E_\theta\alpha_\theta+E_r\alpha_r)}{(C_r+E_r^2)} + \frac{(2(1+C_\varphi)\alpha_\theta+2C_\theta\alpha_r)}{(C_r+E_r^2)}$$

$$D_6 = -\frac{\gamma\left(C_r+E_r^2\right)+2\left(C_r+E_r^2\right)+2E_r^2-2E_rE_\theta-2C_\theta}{C_r+E_r^2},$$

$$D_7 = -\frac{2\gamma(C_\theta+E_rE_\theta)+4(C_\theta+E_rE_\theta)-4E_\theta^2-4E_rE_\theta-2C_\varphi-2}{C_r+E_r^2}, \quad D_8 = -\frac{2(C_\theta+E_rE_\theta)}{C_r+E_r^2}.$$

## References

Dai, H.L. and Wang, X., "Thermo-Electro-Elastic Transient Response", International Journal of Solids and Structures, 42, 1151–1171, 2005.

Ghorbanpour, A., Golabi, S. and Saadatfar, M., "Stress and Electric Potential Fields in Piezoelectric Smart Spheres", Journal of Mechanical Science and Technology, 20, 1920–1933, 2006.

Ghorbanpour Arani, A., Kolahchi, R. and Mosallaie Barzoki, A.A., "Effect of Material In-homogeneity on Electro-Thermo-Mechanical Behaviors of Functionally Graded Piezoelectric Rotating Shaft", Applied Mathematical Modeling, 35, 2771–2789, 2011a.

Ghorbanpour Arani, A., Kolahchi, R., Mosallaie Barzoki, A.A. and Loghman, A., "Electro-Thermo-Mechanical Behaviors of FGPM Spheres Using Analytical Method and ANSYS Software", Applied Mathematical Modeling, 36, 139–157, 2011b.

Ghorbanpour Arani, A., Mosallaie Barzoki, A.A., Kolahchi, R., Mozdianfard, M.R. and Loghman, A., "Semi-Analytical Solution of Time-Dependent Electro-Thermo-Mechanical Creep for Radially Polarized Piezoelectric Cylinder", Computer and Structures, 89, 1494–1502, 2011c.

Jaffe, H. and Berlincourt, D.A., "Piezoelectric Transducer Materials", Proceedings of IEEE, 53, 1372–1386, 1965.

Kordkheili, S.A.H. and Naghdabadi, R., "Thermoelastic Analysis of a Functionally Graded Rotating Disk", Composite Structures, 79, 508–516, 2007.

Loghman, A. and Shokouhi, N., "Creep Damage Evaluation of Thick-Walled Spheres Using a Long-Term Creep Constitutive Model", Journal of Mechanical Science and Technology, 23, 2577–2582, 2009.

Loghman, A., Ghorbanpour, A., Amir, S. and Vajedi, A., "Magnetothermoelastic Creep Analysis of Functionally Graded Spheres", International Journal of Pressure Vessele and Piping, 87, 389–395, 2010.

Mendelson, A., "Plasticity: Theory and Applications", Macmillan Company, New York, 1968.

Penny, R.K. and Marriott, D.L., "Design for Creep", Chapman & Hall, London, 1995.

Salehi-Khojin, A. and Jalili, N., "A Comprehensive Model for Load Transfer in Nanotube Reinforced Piezoelectric Polymeric Composites Subjected to Electro-Thermo-Mechanical Loadings", Composite Part B: Engineering, 39, 986–998, 2008.

Tejeet, S. and Gupta, V.K., "Effect of Anisotropy on Steady State Creep in Functionally Graded Cylinder", Composite Structures, 93, 747–758, 2011.

Wang, H.M. and Xu, Z.X., "Effect of Material Inhomogeneity on Electromechanical Behaviors of Functionally Graded Piezoelectric Spherical Structures", Computational Material Science, 48, 440–445, 2010.

Xuan, F.Z., Chen, J.J., Wang, Z. and Tu, S.T., "Time-Dependent Deformation and Fracture of Multi-Material Systems at High Temperature", International Journal of Pressure Vessel and Piping, 86, 604–615, 2009.

You, L.H., Ou, H. and Zheng, Z.Y., "Creep Deformations and Stresses in Thick-Walled Cylindrical Vessels of Functionally Graded Materials Subjected to Internal Pressure", Composite Structures, 78, 285–291, 2007.

Zhou, D. and Kamlah, M., "Room-Temperature Creep of Soft PZT under Static Electrical and Compressive Stress Loading", Acta Materialia, 54, 1389–1396, 2006.